Instabilities in the Rayleigh-Benard-Eckart problem

Hamda Ben Hadid, Walid Dridi, Valéry Botton, Brahim Moudjed, Daniel Henry

Instabilities in the Rayleigh-Bénard-Eckart problem

H. Ben Hadid, W. Dridi, V. Botton, B. Moudjed, and D. Henry*

Laboratoire de Mécanique des Fluides et d'Acoustique, CNRS/Université de Lyon, École Centrale de Lyon/Université Lyon 1/INSA de Lyon, ECL, 36 avenue Guy de Collongue, 69134 Ecully Cedex, France

(Received 20 December 2011; revised manuscript received 11 May 2012; published 11 July 2012)

This study is a linear stability analysis of the flows induced by ultrasound acoustic waves (Eckart streaming) within an infinite horizontal fluid layer heated from below. We first investigate the dependence of the instability threshold on the normalized acoustic beam width H_b for an isothermal fluid layer. The critical curve, given by the critical values of the acoustic streaming parameter, A_c, has a minimum for a beam width $H_b \approx 0.32$. This curve, which corresponds to the onset of oscillatory instabilities, compares well with that obtained for a two-dimensional cavity of large aspect ratio [A_x = (length/height) = 10]. For a fluid layer heated from below subject to acoustic waves (the Rayleigh-Bénard-Eckart problem), the influence of the acoustic streaming parameter A on the stability threshold is investigated for various values of the beam width H_b and different Prandtl numbers Pr. It is shown that, for not too small values of the Prandtl number (Pr > Pr_l), the acoustic streaming delays the appearance of the instabilities in some range of the acoustic streaming parameter A. The critical curves display two behaviors. For small or moderate values of A, the critical Rayleigh number Ra_c increases with A up to a maximum. Then, when A is further increased, Ra_c undergoes a decrease and eventually goes to 0 at $A = A_c$, i.e., at the critical value of the isothermal case. Large beam widths and large Prandtl numbers give a better stabilizing effect. In contrast, for Prandtl numbers below the limiting value Pr_l (which depends on H_b), stabilization cannot be obtained. The instabilities in the Rayleigh-Bénard-Eckart problem are oscillatory and correspond to right- or left-traveling waves, depending on the parameter values. Finally, energy analyses of the instabilities at threshold have indicated that the change of the thresholds can be connected to the modifications induced by the streaming flow on the critical perturbations.

DOI: 10.1103/PhysRevE.86.016312 PACS number(s): 47.20.Bp, 47.20.Ft, 47.11.Kb

I. INTRODUCTION

Acoustic streaming is a stationary (time-independent) flow occurring in fluids (gases or liquids) subjected to a high-intensity sound field [1]. Acoustic streaming is relevant to some industrial applications such as the pumping of fluids in microflow systems [2] or the mixing of liquids in a closed container (confined medium), which could be of a high efficiency when the flow of the acoustic streaming is used in an adequate pattern [3]. Acoustic streaming is also well known for its transport properties: the fluid flows without any external mechanical contact and can enhance rate-limited processes such as diffusion or heat and mass transfer.

Acoustic streaming is a nonlinear effect that owes its origin to the action of the Reynolds stresses (mean momentum flux due to the ultrasound wave) and the dissipation of the acoustic energy flux [1,4]. This dissipation could be connected to the presence of boundaries and generate what is called Rayleigh-Schlichting streaming, or it could be related to the attenuation of the wave in the bulk fluid and generate Eckart streaming. For the Eckart acoustic streaming we will consider here, the fluid flows away from the ultrasound source in the same direction as the ultrasound wave propagation. The hydrodynamic characteristics of the flow are dictated by the acoustic intensity excitations. Low acoustic intensity excitations generate low-speed flows, and high acoustic intensity excitations generate high-speed flows. If the fluid is bounded by solid walls, the geometric parameter of importance is the relative width of the acoustic beam compared to the fluid layer depth.

Despite the thorough characterization of fluid motions in the Eckart as well as in the Rayleigh-Schlichting streaming situations, to our knowledge there is no work dealing with the stability of such flows including convective heat transfer between horizontal heated plates, but only some studies on the interaction between the streaming flows and the heat transfer. In heated situations, the Prandtl number ($\mathrm{Pr} = \nu/\kappa$) appears as a nondimensional characteristic parameter for the system. Vainshtein *et al.* [5] analytically investigated the effect of Rayleigh-Schlichting streaming on the heat transferred between two horizontal parallel plates that are kept at different temperatures (hot plate above). They found a marked enhancement of the heat transfer due to the Rayleigh streaming and derived asymptotic relations expressing the mean Nusselt number variations. Hyun *et al.* [6] performed experimental and numerical studies to measure the enhancement of the convective heat transfer due to acoustic streaming induced by a vibrating beam (Rayleigh-Schlichting streaming). Their results obtained for a heat transfer from above show that, for an open gap, a vibrating beam at 28.4 kHz with a vibration amplitude of 10 μm causes after 4 min a temperature drop of 30 °C, and with a vibration amplitude of 25 μm the maximum temperature drop reaches 40 °C. In a closed gap, the achieved temperature drop is 10% less than for the open gap. The numerical calculations are able to reproduce the acoustic streaming flow and quantitatively confirm the drop in the temperature observed when the acoustic vibrations are applied. Some other studies considered the heat transfer in air between a lower hot plate and an upper cold plate, but still for acoustic standing waves (Rayleigh-Schlichting streaming).

*daniel.henry@ec-lyon.fr

Nabavi *et al.* [7] experimentally studied the modifications induced on the streaming velocity fields by such differentially heated horizontal walls. They found that when the temperature difference is increased, the streaming velocities are increased too and the originally symmetric streaming vortices are deformed to give asymmetric vortices. Aktas and Ozgumus [8] numerically studied a similar configuration with a two-dimensional approximation. They point out that the transverse temperature gradient strongly affects the acoustic streaming structures and velocities. They also mention an enhancement of the overall heat transfer due to the acoustic streaming. Finally, we have to mention the recent studies concerning Eckart streaming applied in a side-heated cavity, a situation often referred to as the Bridgman configuration in the field of crystal growth [9,10].

In this study, we are concerned with the stability of the Rayleigh-Bénard configuration modified by a forced flow induced by Eckart streaming. This problem is a general theoretical issue and at the same time it could be interesting for different applications such as crystal growth, heat transfer between plates, and Soret separation devices. For this study, we consider a fluid layer of height h heated from below and subject to a constant pressure radiation force caused by an ultrasound beam of width $h_b < h$ oriented along the horizontal x axis. Without acoustic streaming, the Rayleigh-Bénard base state consists of a stagnant fluid layer with a linear temperature variation from the hot bottom to the cold top, and the first instability involves a transition to a steady flow. In our case, the base state still involves the linear vertical temperature variation, but it also comprises a horizontal velocity profile generated by Eckart streaming. The linear stability analysis of this base state has been carried out using accurate numerical methods to determine the neutral curves with minimization with regard to the wave number and then to find the variation of the critical parameter, namely the critical Rayleigh number Ra_c, as a function of the acoustic intensity parameter A for given normalized beam widths H_b. We have extended our results to different values of the Prandtl number and performed energy analyses in order to highlight the stabilizing mechanisms.

II. GOVERNING EQUATIONS

We first consider a rectangular cavity of height h and length l (aspect ratio $A_x = l/h$) filled with a homogeneous Newtonian fluid and subject to a vertical temperature gradient and to the effect of an ultrasound source located in the middle of the left end wall of the cavity. The ultrasound waves propagate in the horizontal x direction inside a beam of characteristic width h_b ($h_b < h$) in the vertical y direction (negligible divergence of the beam [9]). The right end wall of the cavity is an absorber, so that the ultrasound waves are traveling waves. The body force due to the attenuation of the wave is equal to the spatial variation of the Reynolds stress. It is given by Nyborg [1] as $F = -\rho\langle(u_1\cdot\nabla)u_1 + u_1(\nabla\cdot u_1)\rangle$, where ρ is the constant equilibrium density, u_1 is the fluctuating velocity in the sound wave, and $\langle\rangle$ means a time average over a large number of cycles. For a plane wave propagating in the x direction, this body force is oriented in the x direction and its intensity is given by $F = \rho\gamma V_a^2 e^{-2\gamma x}$, where γ is the sound wave spatial attenuation factor and V_a is the sound wave velocity amplitude. Now, provided the attenuation of the wave is sufficiently weak, the body force can be considered as constant inside the beam ($F = \rho\gamma V_a^2$) and zero outside. The top and bottom horizontal walls are perfectly conducting and held at different temperatures, respectively T_c and T_h with generally $T_h > T_c$, whereas the vertical walls are adiabatic. We assume that the physical properties of the fluid are constant (kinematic viscosity ν, thermal diffusivity κ, density ρ) except for the fluid density in the buoyancy term, which obeys the Boussinesq approximation, $\rho = \rho_0[1 - \beta(\bar{T} - T_m)]$, where β is the thermal expansion coefficient and $T_m = (T_c + T_h)/2$ is a reference temperature. Using h, h^2/ν, ν/h, and $(T_h - T_c)$ as scales for length, time, velocity, and temperature, respectively, the governing equations that are the Navier-Stokes equations coupled to the energy equation can be written in a dimensionless form as

$$\nabla\cdot\boldsymbol{V} = \boldsymbol{0}, \tag{1}$$

$$\frac{\partial\boldsymbol{V}}{\partial t} + (\boldsymbol{V}\cdot\nabla)\boldsymbol{V} = -\nabla P + \nabla^2\boldsymbol{V} + \frac{\mathrm{Ra}}{\mathrm{Pr}}\,T\,\boldsymbol{e_y} + f(y)\,\boldsymbol{e_x}, \tag{2}$$

$$\frac{\partial T}{\partial t} + (\boldsymbol{V}\cdot\nabla T) = \frac{1}{\mathrm{Pr}}\,\nabla^2 T, \tag{3}$$

where the dimensionless variables are the velocity vector [$\boldsymbol{V} = (U,V)$], the pressure P, and the temperature T defined by $T = (\bar{T} - T_m)/(T_h - T_c)$. $f(y) = A\,\delta_b$ is the dimensionless force inducing the acoustic streaming (deduced from F), and δ_b is a function of the y coordinate; its value is 1 inside the acoustic beam and 0 outside. In these equations, $\mathrm{Ra} = \beta\, g(T_h - T_c)h^3/\kappa\nu$ is the Rayleigh number, $\mathrm{Pr} = \nu/\kappa$ is the Prandtl number, and $A = \gamma V_a^2 h^3/\nu^2$ is the acoustic streaming parameter. The dimensionless beam width is given by $H_b = h_b/h$.

III. ONE-DIMENSIONAL MODEL: BASIC FLOW

The one-dimensional model corresponds to an infinite horizontal liquid layer of thickness h subject to ultrasound acoustic waves propagating in the x direction inside a beam of width h_b. We assume that the characteristics of the acoustic and hydrodynamic fields remain unchanged along the x direction in such a way that their dependence on the x coordinate can be neglected. For an isothermal liquid layer ($\mathrm{Ra} = 0$), the system (1)–(3) reduces to a system similar to that already used by Rudenko and Sukhorukov [11] for a cylindrical configuration or by Dridi *et al.* [10]. This system is given by

$$\frac{d^2U_0}{dy^2} = f(y) - \frac{\partial P}{\partial x} \quad\text{and}\quad \frac{\partial P}{\partial y} = 0, \tag{4}$$

$$U_0|_{y=0} = U_0|_{y=1} = 0 \quad\text{and}\quad \left.\frac{dU_0}{dy}\right|_{y=0.5} = 0, \tag{5}$$

where $U_0 = U_0(y)$ is the dimensionless base-state acoustic streaming velocity directed along x. Under these conditions and assuming mass conservation, the system admits a unidi-

rectional parallel flow solution:

$$U_0(y) = -\frac{A}{4} H_b y\left[\left({H_b}^2 - 3\right) y - \left({H_b}^2 - 1\right)\right] \quad \text{for} \quad 0 \leqslant y \leqslant 0.5 - H_b/2, \tag{6}$$

$$U_0(y) = -\frac{A}{8}(H_b - 1)^2[2(H_b + 2)(y^2 - y) + 1] \quad \text{for} \quad 0.5 - H_b/2 \leqslant y \leqslant 0.5 + H_b/2, \tag{7}$$

$$U_0(y) = -\frac{A}{4} H_b\,(y - 1)\left[\left({H_b}^2 - 3\right) y + 2\right] \quad \text{for} \quad 0.5 + H_b/2 \leqslant y \leqslant 1. \tag{8}$$

Note that the magnitude of the streaming velocity is a function of the beam width H_b and is proportional to the acoustic streaming parameter A.

When a temperature difference is applied between the upper and lower plates, a conductive temperature profile linear in y is created, given in its dimensionless form by $T_0(y) = 0.5 - y$. This basic temperature profile will not modify the basic velocity profile created by acoustic streaming.

IV. NUMERICAL METHODS

The two-dimensional calculations were performed with the spectral element code with continuation techniques developed by Henry and Ben Hadid [12]. Both the two-dimensional steady flow solutions taking into account the acoustic force and the transition thresholds to oscillations were obtained with this code.

For the one-dimensional approach, we considered the basic state corresponding to the acoustic streaming flow with velocity $U_0(y)$ and the temperature profile $T_0(y)$ that is created in the fluid layer between the infinite plates at $y = 0$ and 1. Let (u,v) be the components of a two-dimensional velocity perturbation $\boldsymbol{v}$ and let θ be the temperature perturbation. The stability of the basic state is examined by disturbing all dependent variables, linearizing the governing equations with respect to the perturbations, and introducing normal mode perturbations given by $(\boldsymbol{v},p,\theta)(x,y,t) = (\boldsymbol{v},p,\theta)(y)\exp(\sigma t + i\alpha x)$, where $\alpha = 2\pi/\lambda$ is the real wave number and λ is the wavelength in the x direction, $\sigma = \sigma_r + i\omega$ is a complex eigenvalue (the real part of which, σ_r, is an amplification rate and the imaginary part, ω, is an oscillation frequency), and ω/α is the phase speed. With the characteristic scales defined above, the pertinent system of equations and boundary conditions describing the evolution of the perturbations may be written as

$$i\alpha u + Dv = 0, \tag{9}$$

$$\sigma u + i\alpha U_0 u + (DU_0)v = -i\alpha p + (D^2 - \alpha^2)u, \tag{10}$$

$$\sigma v + i\alpha U_0 v = -Dp + (D^2 - \alpha^2)v + \frac{\mathrm{Ra}}{\mathrm{Pr}}\theta, \tag{11}$$

$$\sigma\theta + i\alpha U_0\theta - v = \frac{1}{\mathrm{Pr}}(D^2 - \alpha^2)\theta, \tag{12}$$

where $D = \partial/\partial y$ indicates a differentiation with respect to y. The boundary conditions are $u = v = \theta = 0$ at the solid walls. The system of Eqs. (9)–(12) is discretized by the spectral Tau Chebyshev method already described in Kaddeche *et al.* [13]. The resulting generalized algebraic eigenvalue problem is numerically solved by the QZ eigenvalue solver of the Numerical Algorithms Group (NAG) library. A sufficiently large number of Chebyshev polynomials (taken as 81 in this study) is needed to ensure the required numerical accuracy when acoustic streaming is involved. According to the linear theory, the flow is stable if, for given values of H_b, A, and Ra, the amplification factor σ_r is negative for all values of α. Conversely, the flow is unstable if σ_r is positive for some values of α. The states for which the amplification factor is zero are called states of neutral stability. Finally, the neutral state for which the governing parameter, A or Ra, is minimum as a function of α is called the critical state. Note that our results have been checked by comparison with a completely different pseudospectral collocation method using Chebyshev series and developed on MATLAB.

V. KINETIC ENERGY BUDGETS

To better understand the stabilizing or destabilizing mechanisms that will affect the Rayleigh-Bénard situation when acoustic streaming is applied, we will perform kinetic energy analyses based on the critical eigenvectors at threshold. The equations of fluctuating kinetic energy budget are derived from the linear stability equations (10) and (11): Eq. (10) is multiplied by u^* and Eq. (11) by v^*; we then add them and take the real part (Re and the superscript $*$ denote the real part and the complex conjugate, respectively).

The equation expressing the rate of change of the fluctuating kinetic energy (defined as $k = \boldsymbol{v}\boldsymbol{v}^*/2$) is given by

$$\frac{\partial k}{\partial t} = \sigma_r\,(uu^* + vv^*) = k_s + k_d + k_b + k_p, \tag{13}$$

where $k_s = \mathrm{Re}[-v(DU_0)u^*]$ represents the production of fluctuating kinetic energy by shear of the basic flow, $k_d = \mathrm{Re}[(D^2u)u^* + (D^2v)v^* - \alpha^2(uu^* + vv^*)]$ represents the viscous dissipation of fluctuating kinetic energy, $k_b = \mathrm{Re}[(\mathrm{Ra}/\mathrm{Pr})\theta v^*]$ represents the production of fluctuating kinetic energy by buoyancy, and $k_p = -\mathrm{Re}[i\alpha pu^* + (Dp)v^*]$ represents the redistribution of fluctuating kinetic energy by the pressure fluctuations. We can also define the total (or volume integral) fluctuating kinetic energy as $K = \int_y k\,dy$. The rate of change of K is given by an equation similar to Eq. (13), which involves the volume integral energy terms (denoted by K),

$$\frac{\partial K}{\partial t} = K_s + K_d + K_b. \tag{14}$$

Note that the volume integral pressure term is zero and has therefore not been included in Eq. (14). At threshold, the critical eigenvector is associated with an eigenvalue of zero real part. This implies that $\partial k/\partial t$ and $\partial K/\partial t$ are both equal to zero at marginal stability. K_d is stabilizing by nature and is thus a negative term. The kinetic energy equations are then normalized by $|K_d|$. At threshold, and if the normalized terms are denoted with a prime, we get

$$k_s' + k_d' + k_b' + k_p' = 0 \tag{15}$$

and

$$K_s' + K_b' = 1. \tag{16}$$

For any instability at its critical threshold, the calculation of all the individual total energy contributions [Eq. (16)] by using the corresponding critical eigenvector enables us to determine which term plays a dominant role in triggering the instability through production of fluctuating energy. The corresponding spatial fields [Eq. (15)] can in turn be analyzed to locate the production regions.

A complementary approach is based on the expression of the critical Rayleigh number as a function of energetic contributions. For that, we use the fact that the expression of K_b' depends linearly on Ra. At the threshold, we can write $K_b' = \mathrm{Ra}_c K_b''$. And from Eq. (16), we get $\mathrm{Ra}_c K_b'' = 1 - K_s'$, which, for $A = 0$, i.e., in the pure buoyancy case, gives $\mathrm{Ra}_0 K_{b_0}'' = 1$, where the subscript 0 refers to the case $A = 0$ and $\mathrm{Ra}_0 = \mathrm{Ra}_c(A = 0)$. Finally, the ratio of these two equations gives

$$\frac{\mathrm{Ra}_c}{\mathrm{Ra}_0} = \frac{\overbrace{(1 - K_s')}^{R_s}}{\underbrace{\left(K_b''/K_{b_0}''\right)}_{R_b}}, \tag{17}$$

which indicates that the variation of Ra_c with A can be expressed through the ratio of the two quantities, R_s and R_b, the first quantity being connected to the shear of the basic flow due to acoustic streaming and the second quantity to buoyancy. For $A = 0$, R_s and R_b are equal to 1 and $\mathrm{Ra}_c = \mathrm{Ra}_0$. Note finally that U_0 is proportional to A and can be written as $U_0 = AU_{0_A}$. As a consequence we can also define K_s'', which is such that $K_s' = AK_s''$.

VI. RESULTS

The instability of the Rayleigh-Bénard problem ($A = 0$) is one of the prototype problems in laminar transition, and it has been studied extensively. In this case, the critical value of the Rayleigh number is $\mathrm{Ra} = 1707.762$ and the critical wave number is $\alpha = 3.117$. We are concerned in this study with the effect of a slight longitudinal confinement on the stability of the Eckart streaming flow in a layer, and also the modifications the Eckart flow is able to introduce in the stability of the Rayleigh-Bénard problem.

A. Isothermal fluid (Ra = 0)

Without thermal heating ($\mathrm{Ra} = 0$), steady numerical solutions of the system (1)–(3) in a two-dimensional cavity of aspect ratio $A_x = 10$ have been obtained for different beam widths H_b. The velocity vector plot of the solution obtained for a beam width $H_b = 0.8$ and $A = 5200$ is given in Fig. 1. In this figure, the typical stationary streaming structure of the Eckart flow is shown: in the sound beam, the flow is directed away from the sound source, and in the periphery of the layer, it is directed toward the source. Note also that the vertical velocity is significant only in the end regions where the flow changes direction.

FIG. 1. Velocity vector field for the flow induced by an ultrasound source with $H_b = 0.8$ and $A = 5200$ in a two-dimensional cavity with aspect ratio $A_x = 10$.

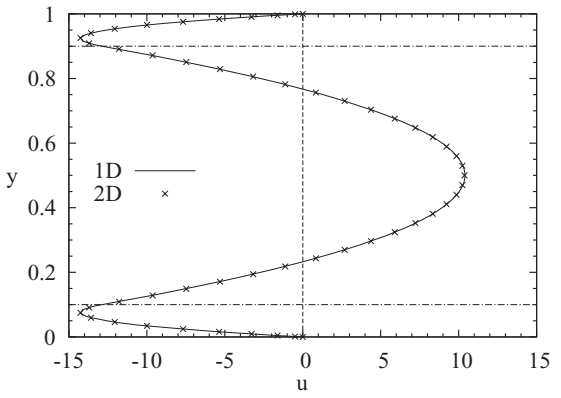

FIG. 2. Comparison between the velocity profiles $u(y)$ obtained analytically with a one-dimensional model [Eqs. (6)–(8), solid curve] or numerically in a two-dimensional cavity with $A_x = 10$ at $x = A_x/2$ (crosses) for the flow induced by an ultrasound source with $H_b = 0.8$ and $A = 5200$. The dot-dashed lines indicate the limits of the acoustic beam.

In Fig. 2, for $H_b = 0.8$ and $A = 5200$, we compare the velocity profile obtained at $x = A_x/2$ in the two-dimensional cavity with $A_x = 10$ to that obtained in an infinite layer and given by Eqs. (6)–(8). It is clear that the two profiles agree very well. In fact, special attention has to be paid to the two-dimensional simulations to get this good agreement. Indeed, if the acoustic force (associated with $\delta_b = 1$) is applied between the two points along the y direction, n_d and n_u, the first idea would be to consider H_b as $y(n_u) - y(n_d)$. In fact this does not work well, as the force does not go sharply to zero at n_d and n_u. Instead, a good agreement is obtained by considering H_b as $[y(n_u) + y(n_u + 1)]/2 - [y(n_d) + y(n_d - 1)]/2$, i.e., the mean value of the distance between the extreme points with $\delta_b = 1$ $[y(n_u) - y(n_d)]$ and the distance between the first neighboring points with $\delta_b = 0$ $[y(n_u + 1) - y(n_d - 1)]$. As the spatial discretization used in our spectral element code is obtained through well defined Gauss-Lobatto-Legendre point distributions, $H_b = 0.8$ (with the previous definition of H_b) cannot be matched precisely for any number of points. Nevertheless, two point distributions with 53 and 87 points along the vertical enable a well defined acoustic beam with $H_b = 0.8$ corresponding to 31 and 51 points in the beam, respectively.

From Fig. 2, which was obtained with the 53-point distribution, we can note that the region where the flow is

oriented in the same direction as the acoustic propagating waves (positive part of the velocity profile) is smaller than the width of the ultrasound beam H_b. In contrast, for small values of the beam width as $H_b = 0.3$, this region is found to be larger than the beam width. Our results also show that for $H_b = 0.8$, the maximum of the streaming velocity is located in the reverse flow, while for small values of the beam width this streaming velocity has a maximum in the central part of the layer. The changes of curvature in the profiles occur in any case at the limits of the beam, and the points where they occur are then displaced toward the walls when the beam width is increased.

The stability of the isothermal and incompressible Eckart-streaming flow, which is governed by the system (9)–(11) with Ra = 0, has been investigated by Dridi *et al*. [10]. These authors determined the critical values of the acoustic streaming parameter, A_c, and the corresponding critical wave number and angular frequency as a function of the beam width H_b. Their results show that the stability of the acoustic stream depends strongly on the beam width H_b. In fact, the critical modes appear to be strongly stabilized for small or large values of H_b, and the more unstable conditions are reached when the beam nearly occupies the third of the liquid layer, i.e., for $H_b \approx 0.32$. For this particular value of the acoustic beam width, the critical parameters are given by Dridi *et al*. [10] as $A_c = 5143$, $\alpha_c \approx 4.5$, and $\omega_c \approx 21$.

The stability of the two-dimensional base flow was considered for an extended cavity of aspect ratio $A_x = 10$. For this large aspect ratio, the parallel one-dimensional flow prevails in the whole cavity except in small regions near the end walls. The calculations with the spectral element code have been done with a fine grid with 101 points in the horizontal direction and 83 points in the vertical direction. Different beam widths have been considered corresponding to an odd number of points along the vertical in the beam increasing from 3 to 51. We have also used the definition of H_b previously given. The critical stability curve corresponding to the first oscillatory transitions is given in the (H_b, A_c) plane in Fig. 3. We see that, owing to the confinement effect, the two-dimensional critical stability curve is located slightly above that of the one-dimensional base flow (infinite horizontal layer). This critical curve clearly shows that the stability of the two-dimensional acoustic stream depends strongly on the beam width H_b and evolves in the same way as the stability of the one-dimensional base flow. We note that for small beam widths corresponding to $H_b \leqslant 0.2$, a steady threshold is found slightly below the oscillatory threshold.

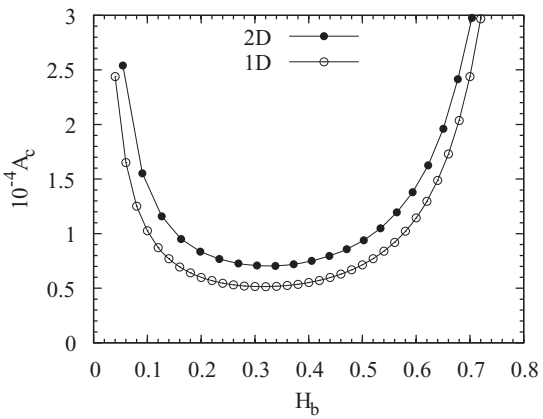

FIG. 3. Critical curves for the onset of oscillatory instabilities in the Eckart flow as a function of the beam width H_b. Comparison between the thresholds A_c obtained for a one-dimensional base flow in an infinite fluid layer (open circles) and for a two-dimensional base flow in a cavity with $A_x = 10$ (solid circles).

B. Heated fluid

We now study the effect of the acoustic stream on the stability of a fluid layer heated from below (Rayleigh-Bénard-Eckart problem). For that, we have to solve the system of hydrodynamic equations (9)–(11) together with the energy equation (12). For a fluid layer between two horizontal, rigid, and perfectly heat conducting boundaries, subject to a vertical temperature gradient, the linear stability theory predicts that such a problem, known as the Rayleigh-Bénard problem, is linearly stable if Ra is less than $\mathrm{Ra}_0 = 1707.762$ and that, when a throughflow is applied as in the Poiseuille-Rayleigh-Bénard problem, the initial increase in the Reynolds number delays the onset of the two-dimensional Rayleigh-Bénard instability (transverse rolls) [14].

The critical stability curves obtained for the Rayleigh-Bénard-Eckart problem are given in Fig. 4 in the $(A, \mathrm{Ra}_c/\mathrm{Ra}_0)$ plane for Pr = 1 and several values of the beam width H_b. The Rayleigh-Bénard stability threshold, which is independent of the Prandtl number, is given by $\mathrm{Ra}_c/\mathrm{Ra}_0 = 1$ and is represented in the figure by a horizontal dashed line. The regions of increased stability will then be above this line. We see that for Pr = 1, the typical shape of the critical stability curves does not change much when the ultrasound width H_b is changed. The critical Rayleigh number Ra_c increases for small A, reaches a maximum Ra_m for A_m, decreases for larger A, and eventually crosses the axis $\mathrm{Ra}_c = 0$ at $A = A_c$ (solid circles). These values $A = A_c$, which correspond to pure hydrodynamic thresholds without any coupling between the velocity field and the thermal field, are exactly those obtained

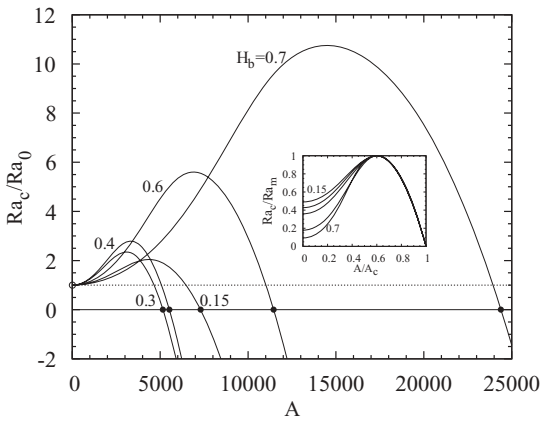

FIG. 4. Critical curves for the onset of instability in the Rayleigh-Bénard-Eckart problem in an infinite layer, expressed as $\mathrm{Ra}_c/\mathrm{Ra}_0$ as a function of A. Different beam widths H_b are considered and Pr = 1. The dashed line (with an open circle) gives the Rayleigh-Bénard threshold and the solid line (with solid circles) gives the Eckart-streaming thresholds A_c. Inset: normalized critical curves expressed as $\mathrm{Ra}_c/\mathrm{Ra}_m$ as a function of A/A_c.

in the case of an isothermal layer by Dridi *et al*. [10] and shown as a function of H_b in Fig. 3. Note also that all the critical curves still exist beyond $A = A_c$ but correspond to negative values of Ra_c. This indicates thresholds of instabilities due to acoustic streaming in situations heated from above that are thus stably stratified.

If there is a typical shape for the critical curves, there is also a clear influence of H_b. The existence range, from 0 to A_c, has a minimum for $H_b \approx 0.32$ and increases for smaller and larger H_b (see the thresholds A_c given in Fig. 3), whereas the maximum critical values Ra_m, reached for $A = A_m$, increase with H_b. Concerning the effective stabilization of the Rayleigh-Bénard situation, we can see that it depends strongly on both the acoustic streaming parameter A and the acoustic beam width H_b. The range of A over which the acoustic streaming has a stabilizing effect (from $A = 0$ to the value of A at which the curves cross the dashed line corresponding to $\mathrm{Ra}_c/\mathrm{Ra}_0 = 1$) also has a minimum close to $H_b = 0.32$ and increases for smaller and larger H_b. (For $\mathrm{Pr} = 1$, this range has an upper bound given by $0 \leqslant A \leqslant A_c$ and corresponding to the domain below the one-dimensional critical curve A_c in Fig. 3.) Large beam widths, however, seem more interesting as the increase of the stabilization range is accompanied by an increase of the stabilization effect (increase of Ra_m). In any case, for a given value of H_b, the best would be to choose a value of A close to A_m. Finally, the inset in Fig. 4 displays the critical curves expressed as $\mathrm{Ra}_c/\mathrm{Ra}_m$ as a function of A/A_c. With such a normalization, we see that the critical curves have similarities: they all reach their maximum for $A/A_c \approx 0.6$, and the decrease from this maximum to zero at $A = A_c$ is similar for all the curves.

The curves for the critical wave number α_c as a function of the acoustic streaming parameter A are given in Fig. 5 for different beam widths and $\mathrm{Pr} = 1$. We can see that for small and moderate beam widths ($H_b \leqslant 0.6$), the wave-number curves for the critical disturbance continuously increase with A (with only some changes of curvature), while for larger beam width ($H_b > 0.6$), the increase of the wave-number curves is interrupted by an intermediate oscillatory variation.

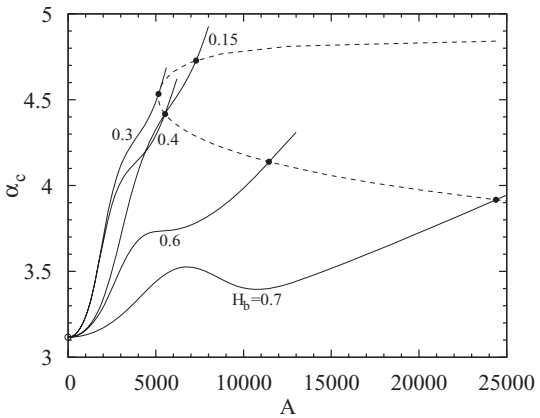

FIG. 5. Critical wave number at the onset of instability in the Rayleigh-Bénard-Eckart problem in an infinite layer, expressed as α_c as a function of A. Different beam widths H_b are considered and $\mathrm{Pr} = 1$. The dashed line with the solid circles gives the critical wave number for the pure Eckart flow.

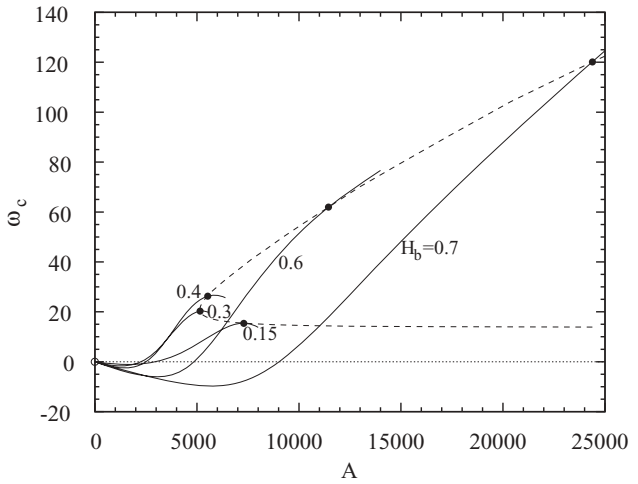

FIG. 6. Critical angular frequency at the onset of instability in the Rayleigh-Bénard-Eckart problem in an infinite layer, expressed as ω_c as a function of A. Different beam widths H_b are considered and $\mathrm{Pr} = 1$. The dashed line with the solid circles gives the critical angular frequency for the pure Eckart flow.

In any case, the curves eventually reach the wave number corresponding to the pure acoustic streaming case ($\mathrm{Ra} = 0$, $A = A_c$), given in the figure by the dashed line with solid circles. Note that for the pure acoustic streaming case, the wave number decreases continuously when increasing the acoustic beam width H_b. Beyond $A = A_c$, i.e., in the domain of negative values of Ra_c, the wave number continues to increase with the increase of A. The observed increase of the wave number corresponds to a decrease of the wavelength, which indicates that shorter perturbation patterns are obtained when A is increased.

The instability found for $A > 0$ corresponds to oscillatory transverse cells. The corresponding critical angular frequency ω_c for these combined Rayleigh-Bénard/Eckart streaming situations is displayed as a function of A for different values of H_b and $\mathrm{Pr} = 1$ in Fig. 6. We see that, as A is increased, the frequency first takes negative values, reaches a minimum, and then increases toward positive values of ω_c, which eventually reach the value corresponding to the pure acoustic streaming case on the dashed line with solid circles. The minimum negative values reached by ω_c increase in absolute value when H_b is increased. These values are around -1.12, -1.68, -2.45, -6.00, and -9.71 for $H_b = 0.15$, 0.3, 0.4, 0.6, and 0.7, respectively. Beyond $A = A_c$, the values of ω_c continue to increase for large beam widths ($H_b \geqslant 0.6$) but quickly decrease for small beam widths and eventually become negative again. The streaming flow then changes the Rayleigh-Bénard steady pattern to traveling waves. Moreover, the negative and positive values of ω_c indicate that these traveling waves can move to the right or to the left depending on the value of A, in contrast with the Poiseuille-Rayleigh-Bénard flow, where the waves can only move downstream. Note that with the choice made in this study, the modes at threshold will vary as $\exp[i(\omega t + \alpha x)]$, so that negative values of ω will correspond to waves traveling to the right (in the positive x direction) whereas positive values of ω will correspond to waves traveling to the left (in the negative x direction).

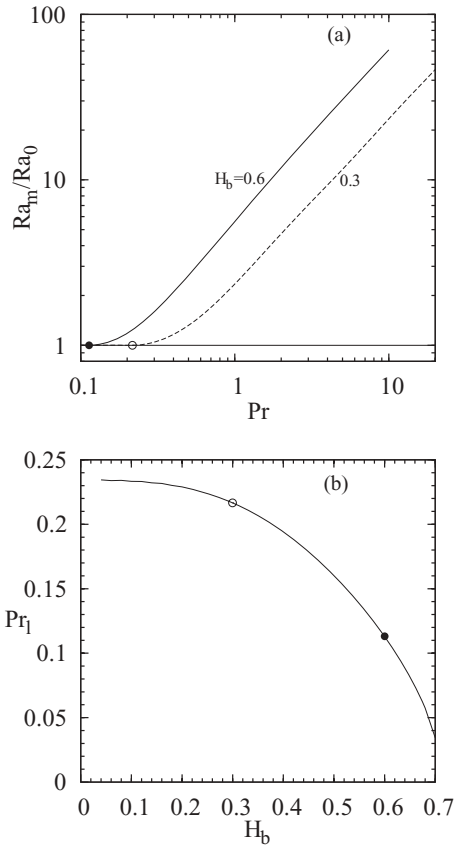

FIG. 7. (a) Maximum value of the Ra_c curve expressed as Ra_m/Ra_0 as a function of the Prandtl number Pr for two beam widths, $H_b = 0.6$ (solid curve and solid circle) and 0.3 (dashed curve and open circle). The circles indicate the limit values Pr_l of the Prandtl number below which the maximum is obtained at Ra_0 for $A = 0$ (no increase of Ra_c in these cases). These limit values Pr_l are given as a function of the beam width H_b in (b).

We found a mistake in Dridi *et al.* [10] where, with the same notations, the negative (positive) values of ω have been wrongly associated with left- (right-) traveling waves.

The previous results have been obtained for a specific value of the Prandtl number, Pr = 1. As we know that these results, contrary to the pure Rayleigh-Bénard situation, depend on the Prandtl number, it would be interesting to have some indications on the effect of Pr. For that, rather than to compute again critical curves that would all begin at Ra_0 for $A = 0$ and end at $Ra_c = 0$ for $A = A_c$, we chose to focus on the maximum value Ra_m reached for $A = A_m$. The variation with Pr of this maximum value given as Ra_m/Ra_0 is shown in Fig. 7(a) for two values of the beam width H_b. We see that for both beam widths, we have an increase of Ra_m with Pr, indicating a better stabilizing effect. Moreover, this increase is linear for large values of Pr (for about $Pr \geqslant 1$ for $H_b = 0.6$ and $Pr \geqslant 5$ for $H_b = 0.3$). Conversely, Ra_m will decrease with decreasing Pr and will eventually reach Ra_0 at some limiting value Pr_l of the Prandtl number (given by circles in the figure). This means that for Pr numbers below this limiting value Pr_l, there will be no more increase of the thresholds Ra_c with A and then no more stabilizing effect induced by acoustic streaming on the Rayleigh-Bénard situation. We have calculated the variation of this limiting value Pr_l with the beam width H_b. The results are shown in Fig. 7(b). We see that Pr_l decreases as H_b is increased, which means that larger beam widths enable stabilizing effects in a larger range of Pr values. The curve of Pr_l is difficult to calculate for low values of Pr_l. Nevertheless, the curve seems to go to zero for $0.7 < H_b < 0.72$. All this indicates that for low Prandtl number fluids (for example $0.01 \leqslant Pr \leqslant 0.03$), a stabilizing effect is difficult to obtain, but it ought to be obtained for very large beam widths as $H_b \geqslant 0.72$. For small beam widths, the curve seems to reach an asymptotic value $Pr_l \approx 0.235$. This indicates that for values of Pr larger than 0.235, a stabilizing effect can be obtained for any beam width. Note finally that during the decrease of Ra_m with decreasing Pr, the associated value A_m (which gives the position of this maximum) remains roughly constant before a strong decrease to zero when the Prandtl number approaches Pr_l.

C. Kinetic energy analyses

To better understand the stabilizing effect that can be induced by acoustic streaming in the Rayleigh-Bénard situation, we performed kinetic energy analyses of the instabilities using the different kinetic energy budgets presented in Sec. V. We first present the results obtained for Pr = 1. We then extend our analysis to other values of Pr.

1. Cases with Pr = 1

As the critical curves have similar characteristics for Pr = 1, we will mainly focus our analysis on the case corresponding to $H_b = 0.3$. For any instability at its critical threshold, the different contributions to the kinetic energy budgets are calculated by using the corresponding critical eigenvector. Such critical eigenvectors are shown in Fig. 8 in the case $H_b = 0.3$ and Pr = 1 for $A = 0$ (left plots) and $A = 3000$ (right plots). We give two-dimensional plots in the vertical (x, y) plane along a wavelength λ of the perturbation, and these plots show the velocity vector field (upper plots) and the isovalues of the temperature field (lower plots). We see that the critical eigenvector is much changed when acoustic streaming is applied: the roughly circular rolls of the Rayleigh-Bénard instability are deformed with acoustic streaming, and the very

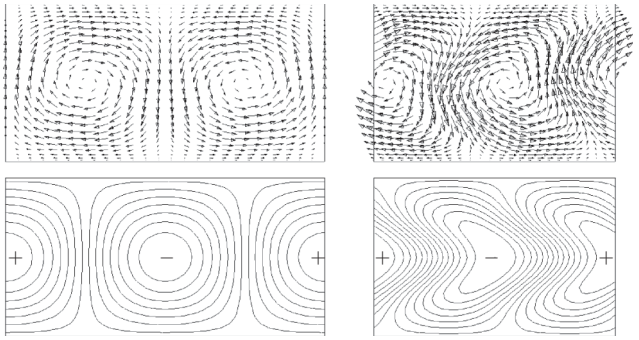

FIG. 8. Critical eigenvectors obtained for $H_b = 0.3$, Pr = 1, $A = 0$ (real eigenvector, left plots), and $A = 3000$ (real part of the complex eigenvector, right plots). The velocity vector field is plotted in the upper part and the isovalues of the temperature field in the lower part. The plots are given in the vertical (x, y) plane along a wavelength λ of the perturbation.

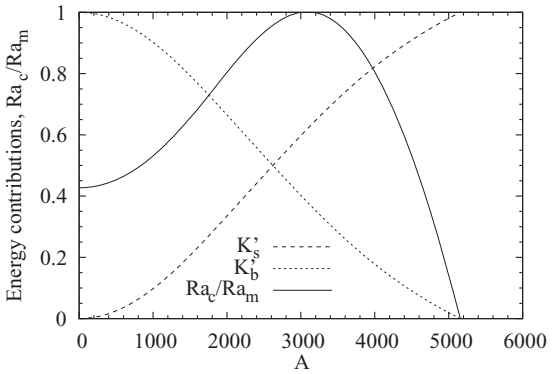

FIG. 9. Variations of the contributions to the total fluctuating kinetic energy budget [K_s' (shear, long-dashed curve), K_b' (buoyancy, short-dashed curve)] for the critical perturbations at threshold as a function of the acoustic streaming parameter A for $H_b = 0.3$ and $\mathrm{Pr} = 1$. The corresponding variation of $\mathrm{Ra}_c/\mathrm{Ra}_m$ (solid curve) is also given.

symmetric temperature perturbation patterns evolve toward arrowhead shapes. Note that the eigenvector obtained for $A = A_c$ is very similar to that shown for $A = 3000$.

The variations with A of the different contributions to the total kinetic energy budget at threshold [Eq. (16)] are shown in Fig. 9 for $H_b = 0.3$ and $\mathrm{Pr} = 1$. We see that both buoyancy and shear terms are destabilizing (positive values), and together they balance the stabilizing dissipation term (negative values). The shear term K_s' increases from 0 at $A = 0$ to 1 at $A = A_c$, while the buoyancy term K_b' decreases from 1 to 0. This indicates that the instability evolves regularly from buoyancy induced at $A = 0$ to shear induced at $A = A_c$. At $A = A_m$, corresponding to the maximum value of the critical Rayleigh number Ra_m, the shear contribution is already larger than the buoyancy contribution.

The spatial fields associated with these kinetic energy contributions and involved in the local kinetic energy budget [Eq. (15)] are shown as y profiles given for different values of A in Fig. 10. For $A = 0$ (thick solid lines), we see the

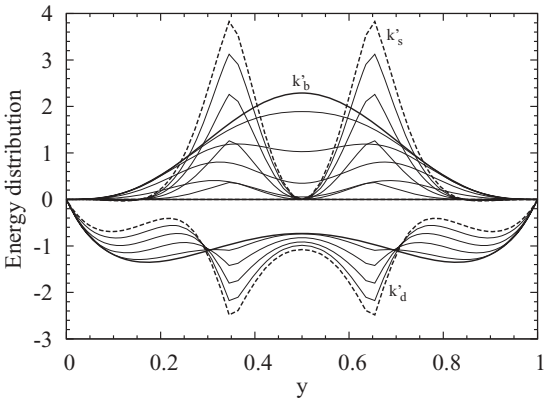

FIG. 10. Contributions to the fluctuating kinetic energy budget: y profiles of the local energy contributions [k_s' (shear), k_b' (buoyancy), k_d' (viscous dissipation)] for the critical perturbations at threshold for $H_b = 0.3$, $\mathrm{Pr} = 1$, and different values of A [$A = 0$ (thick solid lines), $A = 1000$, 2000, 3000, 4000, and $A = A_c = 5157$ (thick dashed lines)].

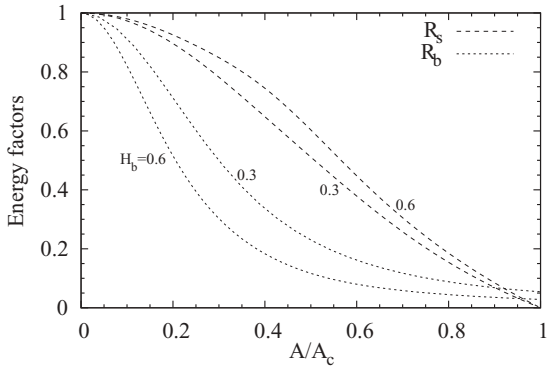

FIG. 11. Variations of the factors R_s (connected to shear, long-dashed lines) and R_b (connected to buoyancy, short-dashed lines) as a function of A/A_c for $H_b = 0.3$ and 0.6 and $\mathrm{Pr} = 1$. R_s and R_b are such that $\mathrm{Ra}_c/\mathrm{Ra}_0 = R_s/R_b$.

strong destabilizing contribution of buoyancy at the center of the layer and the stabilizing contribution of the viscous dissipation, principally along the walls. When A is increased, the shear contribution k_s' connected to acoustic streaming appears with two symmetric peaks located at the limits of the acoustic beam ($|y - 0.5| \approx 0.15$), which grow progressively. k_s' is zero at $y = 0.5$ because, due to the symmetry properties of the perturbation velocity field, u is zero at midheight of the layer. The increase of A induces a decrease of the buoyancy contribution and a change of its shape with the appearance of two symmetric maxima. The viscous dissipation contribution also changes with peaks growing at the limits of the acoustic beam. Finally, for $A = A_c$ (thick dashed lines), we have strong shear peaks associated with peaks in the viscous contribution and no further buoyancy contribution. For clarity of the figure, the pressure contribution was not plotted: in all cases, it enables the local energy equilibrium by transferring energy from the production zones to the dissipation zones.

The last approach is based on the expression of the critical Rayleigh number as a function of energetic contributions, with R_s connected to shear and R_b connected to buoyancy [$\mathrm{Ra}_c/\mathrm{Ra}_0 = R_s/R_b$, Eq. (17)]. The variation with A of these two quantities R_s and R_b is shown in Fig. 11 for $\mathrm{Pr} = 1$ and two beam widths $H_b = 0.3$ and 0.6. R_s and R_b decrease continuously as A is increased, but R_s decreases from 1 for $A = 0$ to 0 for $A = A_c$ whereas R_b decreases from 1 to 0.0548, a small but nonzero limiting value. Moreover, the initial decrease of R_s is small, corresponding to a small initial shear destabilization, whereas the initial decrease of R_b is strong, corresponding to a strong decrease of the destabilizing buoyancy contribution K_b''. These initial evolutions leading to $R_s >> R_b$ explain the initial increase of Ra_c, i.e., the stabilizing effect. We see that this effect is enhanced for $H_b = 0.6$ compared to $H_b = 0.3$ due to a still slower decrease of R_s and a stronger decrease of R_b. The curves of R_s and R_b eventually cross (which corresponds to $\mathrm{Ra}_c = \mathrm{Ra}_0$), which enables the ultimate decrease of Ra_c toward 0 for $A = A_c$.

The variation of the critical thresholds has been shown to depend on the evolution of R_s and R_b, which are directly connected to K_s' and K_b'', respectively. A detailed analysis of these two energy terms may then be useful. This analysis is

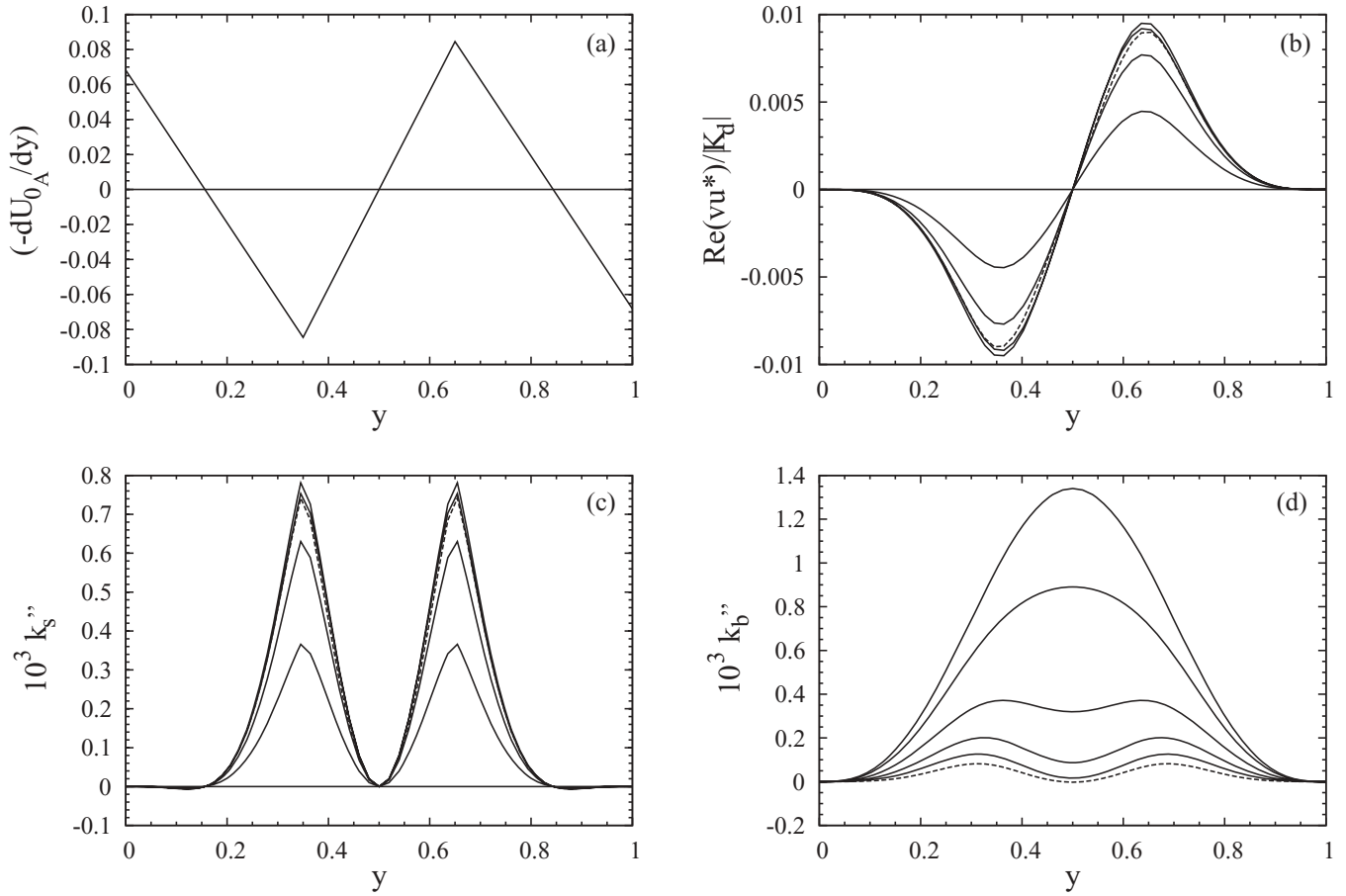

FIG. 12. y profile of $(-dU_{0_A}/dy)$ for $H_b = 0.3$ (a). y profiles of (b) $[\mathrm{Re}(v\,u^*)/K_d]$, (c) k_s'' and (d) k_b'' for the critical perturbations at threshold for $H_b = 0.3$, $\mathrm{Pr} = 1$, and different values of A [$A = 0$ (thick solid lines), $A = 1000$, 2000, 3000, 4000, and $A = A_c = 5157$ (thick dashed lines)]. The shear energy term k_s'' is obtained by multiplying the velocity fluctuation term $[\mathrm{Re}(v\,u^*)/|K_d|]$ by the basic velocity gradient $(-dU_{0_A}/dy)$. $k_s' = A\,k_s''$ is given in Fig. 10.

presented in Fig. 12 through y profiles of important quantities. $K_s' = A\,K_s''$ is the integral of the spatial field $k_s' = A\,k_s''$, and k_s'' [Fig. 12(c)] can be decomposed as a product of two terms, one related to the intrinsic basic flow (independent of A), $(-dU_{0_A}/dy)$ [Fig. 12(a)], and the other related to the velocity perturbations at the critical threshold Ra_c, $[\mathrm{Re}(v\,u^*)/|K_d|]$ [Fig. 12(b)]. K_b'' is the integral of the spatial field k_b'' shown in Fig. 12(d). The profiles of $[\mathrm{Re}(v\,u^*)/|K_d|]$, k_s'', and k_b'' are given for increasing values of A from 0 to A_c. For convenience, the profiles for $A = 0$ are plotted as thick solid lines and those for $A = A_c$ as thick dashed lines.

Concerning the velocity derivative $(-dU_{0_A}/dy)$ [Fig. 12(a)], it is a piecewise linear function in y, which is odd with respect to $y = 0.5$. There is then a change of sign between the upper and lower parts of the layer, but also a change of sign within each half-layer, and the maximum absolute values are reached at the limits of the acoustic beam at $y = 0.5 \pm 0.15$.

The term related to the velocity perturbations, $[\mathrm{Re}(v\,u^*)/|K_d|]$ [Fig. 12(b)], is also odd with respect to $y = 0.5$. It has a positive (negative) peak in the upper (lower) part of the layer, these peaks being centered at the limits of the acoustic beam. This term is zero without acoustic streaming ($A = 0$) due to the symmetry properties of the perturbation flow field in this case (Fig. 8). It first increases as A is increased and then remains approximately constant beyond $A = 3000$ [the maximum amplitude curve in Fig. 12(b) corresponds to $A = 4000$]. k_s'' obtained by multiplying $[\mathrm{Re}(v\,u^*)/|K_d|]$ by $(-dU_{0_A}/dy)$ is then an even function with respect to $y = 0.5$, with two positive peaks centered at the limits of the acoustic beam. Negative values are found closer to the boundaries, in connection with the changes of sign of $(-dU_{0_A}/dy)$, but these values are very small due to the weak values of $[\mathrm{Re}(v\,u^*)/|K_d|]$ in these places. Similarly to $[\mathrm{Re}(v\,u^*)/|K_d|]$, k_s'' has peaks that are zero for $A = 0$, increase as A is increased, and remain approximately constant beyond $A = 3000$. As a consequence, k_s' (which is equal to $A\,k_s''$ and is shown in Fig. 10) is approximately proportional to A beyond $A = 3000$, but it evolves much more slowly for small values of A. Similar variations are found for K_s' (the integral of k_s'), and this explains the small initial decrease of $R_s = 1 - K_s'$.

Finally, the term connected to buoyancy, $k_b'' = \mathrm{Re}\,[(1/\mathrm{Pr})\,\theta\,v^*]$ [Fig. 12(d)], decreases strongly as A is increased. It evolves from the bell-shaped profile at $A = 0$ toward symmetric two-peak profiles. The decrease is particularly strong for small values of A ($A \leqslant 2000$); it is still effective but

smaller for larger values of A until the nonzero limiting profile obtained for $A = A_c$. The strong decrease can be explained by the changes that affect the velocity and temperature perturbations when A is increased (Fig. 8). For $A = 0$, the maximum positive (minimum negative) vertical velocities v are very well correlated with the maximum (minimum) temperature fluctuations θ, in large domains centered at midheight of the layer. On the contrary, when A is nonzero (as can be seen for $A = 3000$), the deformations induced by acoustic streaming on the perturbations lead to v and θ fields, which are much less well correlated. As an example, we can see that the maximum (minimum) temperature fluctuations θ are not associated with strong positive (negative) vertical velocities v.

2. *Other values of* Pr

We have seen that the critical curves are strongly dependent on the Prandtl number: we have an increase of the maximum critical Rayleigh number Ra_m with Pr for not too small Pr values, and below some limiting value Pr_l decreasing critical curves are found. To better understand these behaviors, the energy analysis was performed for $H_b = 0.3$ for two other values of Pr, a stronger value $\mathrm{Pr} = 10$ and a smaller value, below Pr_l, $\mathrm{Pr} = 0.1$. The factors R_s and R_b have been calculated for $\mathrm{Pr} = 0.1$, 1, and 10. We found that the variation with A of the factor R_s does not change much when Pr is changed. On the contrary, the curves of R_b, shown in Fig. 13, are strongly modified when Pr is changed. Compared to the case $\mathrm{Pr} = 1$, the decrease observed for $\mathrm{Pr} = 10$ is much stronger, which explains the very good stabilization observed in this case, whereas the decrease observed for $\mathrm{Pr} = 0.1$ is markedly weaker. For $\mathrm{Pr} = 0.1$, the curve of R_b is also above that of R_s, which explains the constant decrease of the critical curve in this case. Note that the curves of R_b all decrease to a nonzero limiting value for $A = A_c$.

Finally, we want to connect these observations on R_b to particularities of the critical perturbation fields. For that we give the critical velocity and temperature fields obtained for $A = A_c$, $H_b = 0.3$, and $\mathrm{Pr} = 0.1$, 1, and 10 in Fig. 14. For this particular value of A, the instability is purely hydrodynamic

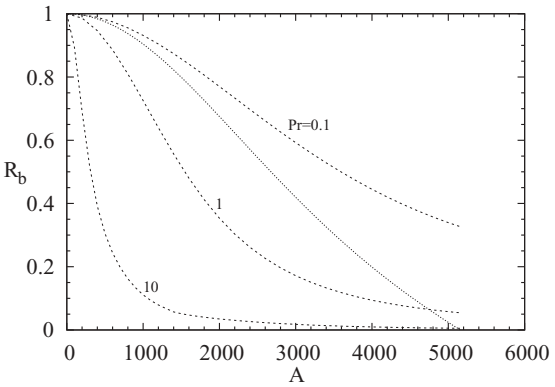

FIG. 13. Variations of the factor R_b (connected to buoyancy, dashed lines) as a function of A (from $A = 0$ to A_c) for $H_b = 0.3$ and different values of Pr. The curve of R_s for $H_b = 0.3$ and $\mathrm{Pr} = 0.1$ (dotted line) is given for comparison.

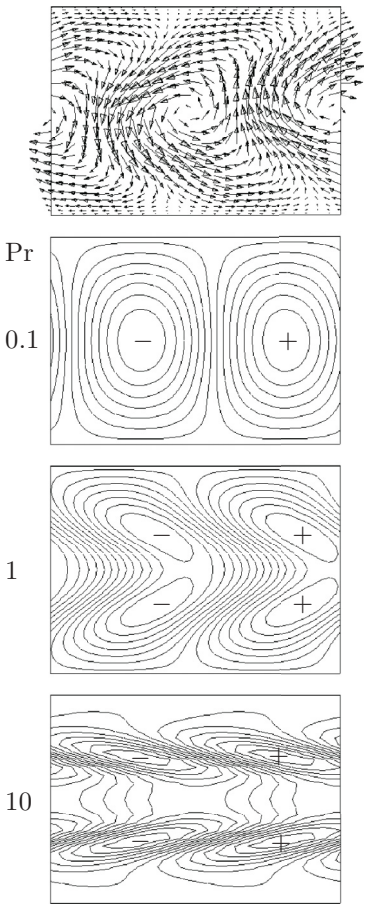

FIG. 14. Real parts of the complex critical eigenvectors obtained for $H_b = 0.3$, $A = A_c$, and different values of the Prandtl number. The velocity vector field does not depend on Pr. The isovalues of the temperature field are given for $\mathrm{Pr} = 0.1$, 1, and 10. The plots are given in the vertical (x, y) plane along a wavelength λ of the perturbation.

and does not depend on Pr. The velocity perturbation is then independent of Pr, whereas the temperature perturbation is the limit perturbation obtained for $A = A_c$ for each value of Pr. We know that the intensity of the R_b factors is connected to the amplitude of the k_b'' profiles, and then to the degree of correlation between the v and θ perturbations. This is what we observe here. For $\mathrm{Pr} = 0.1$, the temperature perturbation field is not much deformed and the correlation between the v and θ perturbations remains good. On the contrary, for $\mathrm{Pr} = 1$, the temperature perturbation field is much deformed with maximums that are no longer at midheight and the correlation is strongly reduced. All this is still accentuated for $\mathrm{Pr} = 10$ leading to a still poorer correlation. We can conclude that the influence of Pr on the critical curves is mainly connected to the changes that affect the temperature perturbation fields.

VII. CONCLUSION

We have presented results of a detailed analysis of the Rayleigh-Bénard-Eckart instabilities for various acoustic beam widths H_b, a wide range of acoustic streaming parameter

A, and different values of the Prandtl number Pr. The analytical solution for the steady-state velocity of a one-dimensional flow resulting from the action of the ultrasound source has been first determined and the profiles thus obtained compare well with the velocity profiles obtained from two-dimensional direct numerical calculations in a long cavity. The destabilizing thresholds A_c of the Eckart flows in such two-dimensional situations are similar to the thresholds of the one-dimensional flow, but a little higher due to the confinement.

Concerning the linear stability results of the Rayleigh-Bénard-Eckart configuration, it has been found that the acoustic streaming flow modifies the stability of the fluid layer heated from below. More precisely, for not too small values of the Prandtl number ($\mathrm{Pr} > \mathrm{Pr}_l$), the onset of instability is delayed when the acoustic streaming is applied, which corresponds to a critical Rayleigh number Ra_c increasing with the acoustic streaming parameter A and thus reaching higher values than the critical value Ra_0 of the Rayleigh-Bénard problem at $A = 0$. In some cases, this stabilization could be very strong, especially for large values of the beam width H_b and large values of the Prandtl number Pr. Nevertheless, increasing A beyond some specific value A_m (mainly depending on H_b) lowers the value of Ra_c, the instability threshold eventually reaching the pure acoustic streaming threshold A_c at $\mathrm{Ra} = 0$. In contrast, for small values of the Prandtl number ($\mathrm{Pr} \leqslant \mathrm{Pr}_l$), there is no stabilizing effect and the thresholds Ra_c decrease from Ra_0 to 0. The limiting value Pr_l has been found to decrease with the increase of H_b, from 0.235 for small H_b to zero for $H_b \approx 0.72$. This indicates that larger beam widths enable stabilizing effects in a larger range of Pr values, and that for $\mathrm{Pr} > 0.235$ or for $H_b > 0.72$, stabilizing effects are always obtained. The instabilities that are triggered correspond to oscillatory transverse rolls, which are characterized by a wave number and an angular frequency depending on A, H_b, and Pr. The main observation is that the angular frequency values change from negative to positive when A is increased, indicating a change from right-traveling to left-traveling waves.

Finally, information on the stabilizing and destabilizing mechanisms has been obtained from the kinetic energy analyses of the instabilities at threshold. When A is increased from 0 to A_c, it is found that the destabilizing buoyancy contribution decreases while the destabilizing shear contribution due to acoustic streaming increases, indicating a continuous change of the instability from thermally induced to shear induced. A deeper analysis shows that the initial increase of the instability thresholds can be connected to the modifications induced by the streaming flow on the critical perturbations. When the streaming flow is enhanced ($A > 0$), these modifications influence differently the velocity perturbation product ($v\,u$) involved in the shear energy term, which slowly increases, and the perturbation product ($\theta\,v$) involved in the buoyancy energy term, which strongly decreases, and this can be shown to induce the increase of the critical Rayleigh number. The increase of the thresholds with Pr can also be connected to the influence of Pr on the perturbation product ($\theta\,v$).

[1] W. L. Nyborg, in *Nonlinear Acoustics*, edited by M. F. Hamilton and D. T. Blackstock (Academic, San Diego, 1998), p. 207.

[2] K. D. Frampton, S. E. Martin, and K. Minor, Appl. Acoust. **64**, 681 (2003).

[3] C. Suri, K. Takenaka, H. Yanagida, Y. Kojima, and K. Koyama, Ultrasonics **40**, 393 (2002).

[4] J. Lighthill, J. Sound Vib. **61**, 391 (1978).

[5] P. Vainshtein, M. Fichman, and C. Gutfinger, Int. J. Heat Mass Transf. **38**, 1893 (1995).

[6] S. Hyun, D. R. Lee, and B. G. Loh, Int. J. Heat Mass Transf. **48**, 703 (2005).

[7] M. Nabavi, K. Siddiqui, and J. Dargahi, Int. Commun. Heat Mass Transf. **35**, 1061 (2008).

[8] M. K. Aktas and T. Ozgumus, Int. J. Heat Mass Transf. **53**, 5289 (2010).

[9] W. Dridi, D. Henry, and H. Ben Hadid, Phys. Rev. E **77**, 046311 (2008).

[10] W. Dridi, D. Henry, and H. Ben Hadid, Phys. Rev. E **81**, 056309 (2010).

[11] O. V. Rudenko and A. A. Sukhorukov, Acoust. Phys. **44**, 565 (1998) [Akusticheskii Zhurnal **44**, 653 (1998)].

[12] D. Henry and H. Ben Hadid, Phys. Rev. E **76**, 016314 (2007).

[13] S. Kaddeche, D. Henry, and H. Ben Hadid, J. Fluid Mech. **480**, 185 (2003).

[14] X. Nicolas, Int. J. Thermal Sci. **41**, 961 (2002).